Analytical Chemistry Research 5 (2015) 1–8

Contents lists available at ScienceDirect

Analytical Chemistry Research

journal homepage: www.elsevier.com/locate/ancr

Direct electron transfer biosensor for hydrogen peroxide carrying nanocomplex composed of horseradish peroxidase and Au-nanoparticle – Characterization and application to bienzyme systems

Yusuke Okawa *, Naoto Yokoyama, Yoshinori Sakai, Fumiyuki Shiba

Graduate School of Advanced Integration Science, Chiba University, 1-33 Yayoicho, Inage-ku, Chiba 263-8522, Japan

ARTICLE INFO

Article history:
Received 4 March 2015
Accepted 18 May 2015
Available online 23 May 2015

Keywords:
Electrochemical biosensor
Direct electron transfer
Au-nanoparticle
Horseradish peroxidase
Glucose oxidase
Urate oxidase

ABSTRACT

A reagentless electrochemical biosensor for hydrogen peroxide was fabricated. The sensor carries a monolayer of nanocomplex composed of horseradish peroxidase and Au-nanoparticle, and responds to hydrogen peroxide through the highly efficient direct electron transfer at a mild electrode potential without any soluble mediator. Formation of the nanocomplex was studied with visible spectroscopy and size exclusion chromatography. The sensor performance was analyzed based on a hydrodynamic electrochemical technique and enzyme kinetics. The sensor was applied to fabrication of sensors for glucose and uric acid through further modification of the nanocomplex-carrying electrode with the corresponding hydrogen peroxide-generating oxidases, glucose oxidase and urate oxidase, respectively.

1. Introduction

Recent progress in nanomaterials enables us new strategies in a wide field of science and technology. As nanomaterials feature unique surface and electronic characters, they have attracted a strong interest to apply them for fabricating functional systems, of course, within the field of biosensors [1]. Especially, nanoparticles are extensively studied in view of this [2]. For example, nanoparticles as molecular labels, electrode catalysts, and nanoscale connectors between redox enzymes and base electrodes have been reported.

We are interested in the electronic and surface characters of nanoparticles as nanoscale interface for biofunctional molecules. Several workers reported use of Au-nanoparticle (AuNP) for the fabrication of electrochemical biosensors without soluble electron mediators, and demonstrated that AuNPs are expected to present an effective electrochemical interface to some enzymatic reactions [3–6].

In a previous communication, we have briefly reported a novel high performance and reagentless electrochemical biosensor for hydrogen peroxide using combination of horseradish peroxidase (HRP) and AuNP [6]. The sensor is an indium-tin oxide (ITO) electrode carrying a monolayer of nanocomplex composed of an AuNPs and HRP molecules, and is prepared in a very simple manner. The nanocomplex is immobilized through simply drop-casting the nanocomplex dispersion on the electrode. The sensor gives direct electrocatalytic current to H_2O_2 with high electron transfer efficiency at a mild potential without any soluble mediator.

Determination of hydrogen peroxide has been an important topic in very wide fields, such as environmental, pharmaceutical, clinical, and industrial applications, as reported in many works. Our system requires the mild electrode potential comparable to a soluble mediator system [7]. This is a strongly attractive feature for minimizing non-specific electrochemical responses in practical applications. Although there are several reports about the direct electron transfer systems using the combination of the AuNP and HRP [3,8–10], the working electrode potentials were generally more negative, that is, they required a relatively high overpotential for the direct electron transfer to HRP. Recent papers using the combination of HRP and AuNP tend to "hybrid" approaches, that is, the nanoparticles are combined with organic/inorganic materials [11–14]. These approaches mainly aim to enhance the amount of enzyme and/or functional site, and improve the sensitivity and stability. Thus, the working potential of these sensors are not improved relative to the conventional HRP/Au-nanoparticle systems reported. On the other hand, our system features not only

* Corresponding author. Tel.: +81 43 290 3452.
E-mail address: y_okawa@faculty.chiba-u.jp (Y. Okawa).

http://dx.doi.org/10.1016/j.ancr.2015.05.001
2214-1812/

"simplicity" but the extensively improved (i.e. "mild") working potential for H_2O_2 detection.

The improved working potential and high sensitivity for H_2O_2 detection are attractive to fabricate biosensors for oxidase substrates. Oxidases generate H_2O_2 through the oxidation of the substrates by dissolved O_2. The sensitive detection of thus generated H_2O_2 gives sensors for the oxidase substrates by the combination with the oxidase.

In this paper we describe detailed analysis and further application of the above nanocomplex-based sensor. We first describe characterization of the nanocomplex and the immobilized layer. We then discuss the kinetics of the surface process of the sensor response of the nanocomplex-carrying electrode based on a hydrodynamic electrochemical technique and enzyme kinetics. For evaluating the applicability of the proposed sensitive H_2O_2 detection system, we fabricated biosensors for glucose and uric acid by further immobilizing glucose oxidase (GO) and urate oxidase (UO) onto the nanocomplex-carrying electrode, respectively.

2. Experimental

2.1. Materials

Horseradish peroxidase (HRP, EC1.11.1.7, Type VI), glucose oxidase (GO, EC1.1.3.4, from *Aspergillus niger*, Grade II), urate oxidase (UO, EC1.7.3.3, from yeast) was purchased from Sigma, Boehringer Mannheim, and Oriental Yeast, respectively. A series of pullulans from Shodex was used as the molecular weight standards for size exclusion chromatography (SEC). All other chemicals were of reagent grade and used without further purification. Water was purified with deionization and distillation. Indium-tin oxide (ITO) coated glass plates (sheet resistance 10 Ω) and fluoride-doped tin oxide (FTO) coated glass plates (sheet resistance 10 Ω) were from Geomatec and Nippon Sheet Glass, respectively.

2.2. Preparation of nanoparticles, nanocomplex, and electrodes

Quasi-monodisperse AuNPs with an average diameter of 16 nm were prepared with the citrate reduction of 1 mmol L^{-1} $HAuCl_4$ at the boiling temperature [15–17].

A prescribed amount of HRP was dissolved at room temperature in the AuNP dispersion prepared above. A prescribed amount of the mixed solution was cast on the base electrode, and naturally dried below 10 °C to give an HRP–AuNP nanocomplex-carrying electrode.

For the preparation of bienzyme electrodes, the nanocomplex-carrying ITO electrode was first treated with 1% glutaraldehyde solution for 15 min, rinsed with water, and then treated with the enzyme solution for 15 min.

2.3. Methods

Electrochemical measurements were operated with the conventional 3-electrode system with a Toho Giken potentiostat Model 2000 and a Yokogawa Electric Works pen recorder. Hydrodynamic experiments were performed with a rotating Au disc electrode and a Hokuto Denko rotator. A home-made Ag/AgCl electrode (KCl satd.) and a Pt wire were used as reference and counter electrodes, respectively. All experiments were done in a working solution (a 0.1 mol L^{-1} phosphate buffer of pH 6.4) at 25 °C.

Transmission electron microscopic observation was done with JEOL JEM-1200EX and Hitachi Denshi H-7650 electron microscopes.

UV–Vis absorption spectra were obtained with a Shimadzu spectrometer Model UV3100.

Size exclusion chromatography was carried out with Shodex Asahipak GS-620 columns (two columns in series, with a GS-2G 7B pre-column) and a Hitachi HPLC pump Model L-6000. The eluent was a 0.2 mol L^{-1} phosphate buffer (pH 6.4) and the operation was carried out at 50 °C. The detection in a UV region was carried out with a Hitachi diode array detector Model L-3000. The detection in a visible region was carried out with an Ocean Optics diode array spectrophotometer Model USB2000 with a flow-through optical cell.

The dc electrical conductivity of the immobilized layer was measured using an Advantest digital multimeter Model R6871 and a comb-type electrode.

3. Results and discussion

3.1. Characterization of AuNPs and nanocomplex

Fig. 1(A) shows a transmission electron micrograph of the prepared AuNPs featuring the average diameter of 16 nm (17% CV). The visible absorption spectrum of the dispersion was shown in Fig. 1(B), exhibiting typical plasmon absorption at around 520 nm.

When a protein was dissolved in the dispersion, the red shift of λ_{max} was observed. Fig. 1(C) shows change in the λ_{max} as a function of the added HRP concentration. The mixed dispersion includes 6×10^{15} particles L^{-1} of the AuNPs. As the enzyme concentration increases, the λ_{max} increases and shows saturation. The shift indicates the enzyme adsorption on the nanoparticle surface [18], and the saturation of the shift suggests the saturation of the enzyme adsorption.

Fig. 2 shows a typical size exclusion chromatogram for the mixed dispersion of the AuNP and HRP. The dispersion contained a sufficient concentration of HRP (20 μmol L^{-1}) to ensure the saturation of the enzyme adsorption. The detection was done with the absorption at 210 nm. The trace shows three major peaks, A, B and C. The peak C was assigned to citrate originally contained in the reaction mixture from the retention time and the UV absorption spectrum. The insets in Fig. 2 show the absorption spectra corresponding to the peaks A and B, respectively. The molecular weight (pullulan equivalent) of the peak B calculated from the retention time is reasonably agreed with the molecular weight of HRP (44 kDa [19]). Correspondingly, the peak B exhibited absorption maxima at around 210 nm (peptide bond), 280 nm (weak, aromatic amino acid residues), and 400 nm (heme) (see the inset). The peak B corresponds to the (excess) free HRP molecules. The peak A gives the absorption maximum at around 525 nm corresponding to the plasmon absorption of the AuNP, and light scattering towards the UV region. The pullulan equivalent molecular weight of the peak A was 2.0×10^5, and hence, the corresponding hydrodynamic diameter was estimated at 27 ± 2 nm [20]. This value is reasonable as the size of the AuNP (16 nm) with the adsorbed HRP (5 nm [21]) monomolecular layer. We thus concluded that the peak A corresponds to the AuNPs with the adsorbed enzyme monolayer. On the contrary, the AuNPs protected only with citrate (without the adsorbed protein) coagulate and precipitate when the elution buffer is added to the dispersion. The drastic improvement in the dispersion stability is also consistent with the enzyme adsorption.

In general, adsorption behaviors should be essentially discussed through the adsorption isotherm. In Fig. 2, however, we could not evaluate the real equilibrium (non-adsorbed or free) enzyme concentrations in the ordinate. We attempted the determination of the free enzyme concentration in the dispersion containing 6.0×10^{15} particles L^{-1} of the AuNPs and 0.15 μmol L^{-1} (9.2×10^{16} molecules L^{-1}) HRP as follows. The AuNPs were separated from the dispersion and the supernatant was concentrated and analyzed with HPLC (the same setup with the above size exclusion chromatography). The detection limit of the enzyme through

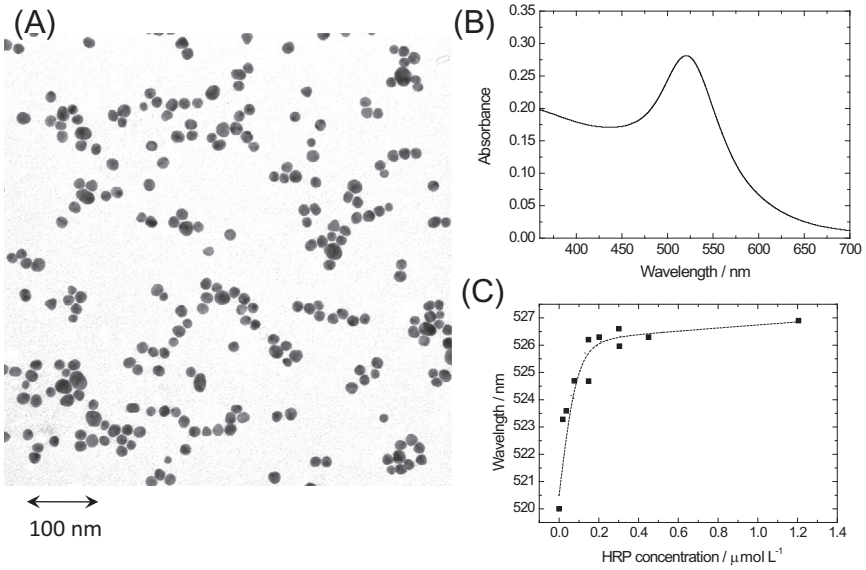

Fig. 1. TEM image (A) and visible absorption spectrum (B) of the AuNP (as-prepared). (C) Change in peak wavelength of plasmon absorption of AuNP with HRP concentration.

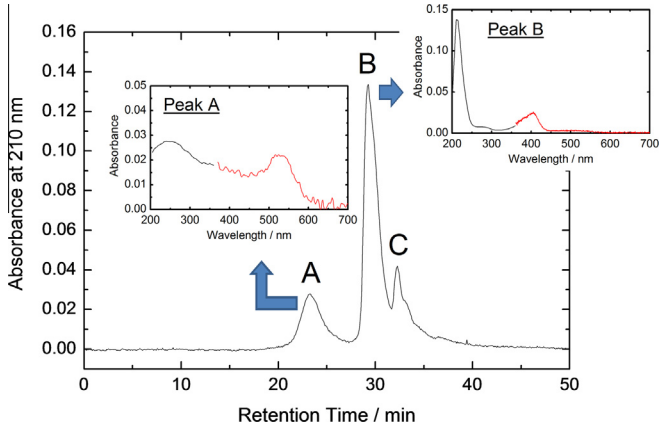

Fig. 2. Size-exclusion chromatographic trace of a HRP/AuNP mixed dispersion. The insets indicate a UV–Vis spectra at the corresponding peaks.

this entire process was 10 pmol, and we could not detect any enzyme from the supernatant. This means that more than 95% of the added enzyme molecules were adsorbed at this enzyme concentration. We thus calculated that 15 molecules of HRP were adsorbed on each AuNP at this condition. Below this added amount level, we can consider the approximately complete adsorption of the enzyme added on the AuNPs. When the enzyme concentration increased, we can detect reasonable amounts of HRP with the above method. The saturated adsorbed amount is estimated at 50 molecules/particle, being geometrically consistent with the respective sizes of the AuNP and HRP molecule.

The monolayer adsorption of an enzyme on a nanoparticle means the formation of a new functional nanocomplex. In the following sections, we discuss the characteristics of the electrodes carrying this nanocomplex.

3.2. Sensor performance and preparative conditions

The above HRP/Au-nanocomplex was easily immobilized on an ITO electrode surface by the simple drop-cast technique. The deposited nanocomplex was sufficiently stable against rinsing with water. The nanocomplex-carrying electrode shows an excellent sensor performance to H_2O_2 without any soluble mediator. We further examined the effect of the base electrode materials on the sensor characteristics using ITO, FTO, and Au as the base electrode.

Fig. 3 shows calibration graphs for the nanocomplex-carrying electrodes of various base electrode materials. All electrodes responded to the addition of H_2O_2 within several seconds under continuous gentle stirring. The ratio of enzyme/AuNP (number base) was 15, and the immobilized density of the nanocomplex was 2.7×10^{11} particles cm^{-2} (the nominal value for the immobilization process). The conditions were the optimized ones based on the investigation described below. The electrode was operated at +0.15 V vs. Ag/AgCl, where the direct electrochemistry of H_2O_2 is not observed for bare and AuNP deposited electrodes. The solution is continuously stirred at ~1 rps and the response time is rather limited with the stirring itself.

The sensor performance depended on the base electrode materials especially in sensitivity, although the current-concentration profiles were geometrically similar in essence. The sensitivity in the case of an FTO base electrode was obviously the lowest among these base electrode materials. It was also found that the nanocomplex was apt to partially peel off from the FTO surface. On the Au electrode, the nanocomplex was stably immobilized

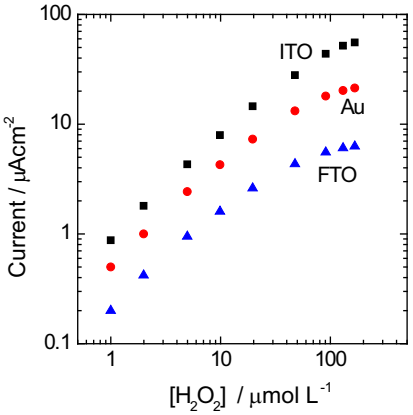

Fig. 3. Typical sensor response of the nanocomplex-carrying electrodes of various materials at +0.15 V vs. Ag/AgCl under continuous stirring (~1 cps); ■, ITO; ●, Au; ▲, FTO. HRP/AuNP ratio = 15:1, immobilized density = 2.7×10^{11} cm^{-2}.

but the sensitivity as the sensor was about half of the ITO electrode. These observations strongly suggest that the nanocomplex effectively connected to the base electrode contributes to the sensor response, and that the contact between the AuNP core of the nanocomplex and the base electrode surface is essentially important for the sensitivity. These results will be discussed in view of the kinetic analysis below. ITO is the best choice for the present nanocomplex system among the electrode materials examined.

Fig. 4(A) shows the sensor response as a function of the HRP/AuNP ratio for ITO electrodes carrying the nanocomplex. The curve shows a maximum at the ratio ~15. When the ratio is larger than ~20, we observed that some of the deposited nanocomplexes peeled off from the electrode. In this region, non-adsorbed enzyme molecules are simultaneously deposited on the electrode. These molecules do not strongly interact with the surfaces of both the AuNPs and the base electrode, but lie between the nanocomplexes and/or between the nanocomplex and the base electrode. When these excess molecules dissolve, a part of the nanocomplexes simultaneously peel off, and hence the sensor response decreases. When the ratio is smaller, the limited amount of the introduced enzyme limits the response. From the stability of the deposited layer and the loaded enzyme amount, we chose the ratio of 15 as the optimum.

Fig. 4(B) shows the sensor response as a function of the loaded density of the nanocomplex on the ITO electrode. In the low density region, the response increases with the increase of the loaded density, but saturates in the high density region. When the loaded amount exceeds a certain value, the nanocomplexes exist as the multilayer. When there is no electrical connection between the nanocomplexes, only the nanocomplex in the first layer can electrically connected to the base electrode, and can contribute to the electrochemical response. We measured the electrical conductivity of the nanocomplex layers deposited on a comb-type electrode. The monolayer and multilayer of the nanocomplexes is highly insulating (at least 10^{10} Ω of the sheet resistance) in a dry nitrogen atmosphere, although a wet air atmosphere gives a measurable conductivity originated by water adsorbed on the protein molecules. We thus concluded that there is no electrical connection between the immobilized nanocomplexes.

Fig. 5 shows a TEM image of the deposited nanocomplex layer of the optimized conditions. The film was peeled off from the electrode for the TEM observation. The particle density of 2.2×10^{11} cm^{-2} was observed from the photographs and reasonably agreed with the loaded density of 2.7×10^{11} cm^{-2}. In this image, we can see that the AuNPs do not contact with each other. This is caused by the adsorbed protein layer (just visible as slight shadow in the TEM images), and is consistent with the results of the electrical conductivity measurement and the HPLC analysis above.

In the immobilized nanocomplex layer, the AuNP cores do not contact with each other, and electrical connection between the nanocomplexes is negligible with this system. The multilayer loading of the nanocomplex is thus ineffective for the higher output current because the nanocomplexes in the lowest layer can only have the electrical connection to the base electrode. As seen in

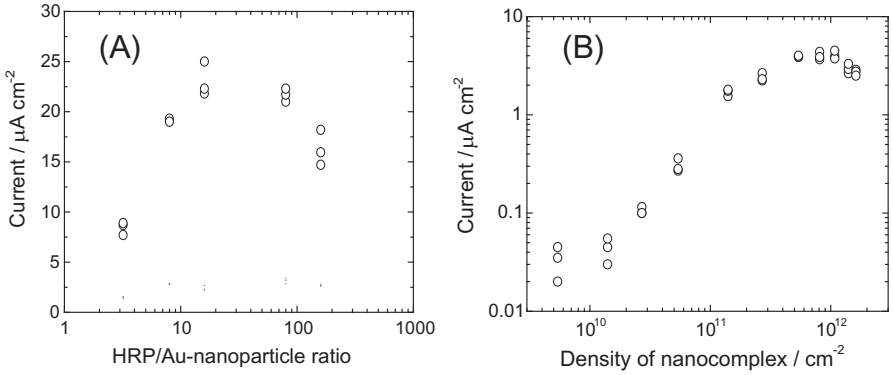

Fig. 4. Sensor response as the functions of (A) the HRP/AuNP ratio (immobilized density = 2.7×10^{11} cm^{-2}; H_2O_2 concentration = 100 mmol L^{-1}) and (B) the immobilized density (right, HRP/Au-nanocomplex ratio = 15:1; H_2O_2 concentration = 10 mmol L^{-1}). Base electrode, ITO.

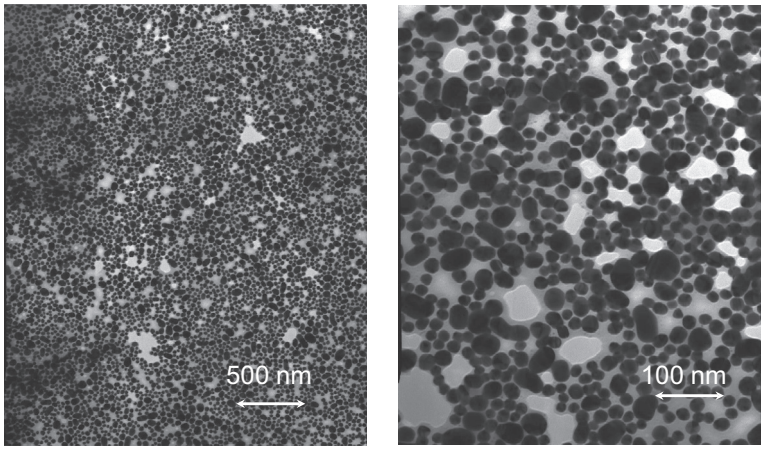

Fig. 5. TEM images of coagulated nanocomplex film peeled off from the electrode. Loaded density = 2.7×10^{11} cm^{-2}.

Fig. 4(B), the response is saturated at $\sim 5 \times 10^{11}$ cm^{-2} level. This corresponds to the completion of the packed monolayer, being consistent with the TEM observation in Fig. 5.

The stability of the electrodes was examined. The electrodes were stored in air under refrigeration below 10 °C when not in use, and the response to 10 μmol L^{-1} H_2O_2 was measured daily. The sensor outputs after the 3 d storage were about 70% of the initial one. The electrodes show good reproducibility and stability under these conditions. However, after the electrode was once used in a high concentration of H_2O_2 (e.g. 1 mmol L^{-1}), the response was suppressed to 50–70% of the original level even when it was again operated in a dilute H_2O_2 solution. When the electrode is operated in such high H_2O_2 concentration conditions, the current response also gradually decreased. This instability is due to the intrinsic nature of HRP [22], and is an essential problem of HRP-based biosensors. However, use of the electrode in these high concentration conditions is a rather special case in bioanalytical applications, and the solution of this problem is beyond the scope of the present work.

3.3. Hydrodynamic electrochemistry and kinetic analysis

The present electrode gave a steady-state current to the substrate when the solution was continuously stirred. When the stirring stopped, the current gradually decreased, and when the stirring restarted, the current recovered to the original level. The result means that the substrate supply to the electrode is one of rate limiting steps in the sensor response.

We should analyze the surface process to characterize the behavior of the nanocomplex separately from the mass transfer process. We applied a hydrodynamic technique, that is, the rotating disc electrode (RDE) method to evaluate separately these processes. In this experiment, an Au disc electrode was employed because of the availability of the electrode whose geometry is suitable for the RDE experiment. The rotation speed dependency of the sensor response was examined in the electrolyte containing various concentrations of the substrate. The sensor output clearly increased as the rotation speed increased. Fig. 6(A) shows Koutecky–Levich plots of the output current at various substrate concentrations. Each plot gives a reasonable straight line with a certain value of the intercept. This means the mass transfer of the substrate and the surface charge transfer process are both the rate determining steps. The slope of each plot gives an essentially identical diffusion constant of 7.1×10^{-6} cm^2 s^{-1} that is reasonable for the one of H_2O_2.

The intercept of Koutecky–Levich plot gives the net charge transfer rate without the mass transfer effect and we can exactly evaluate the kinetics of the surface process. Fig. 6(B) shows a typical H_2O_2 dependence of the surface reaction rate determined by the above analysis. This figure is an ideal calibration graph under the conditions where the mass transfer is infinitely rapid and only the surface reaction is rate-determining. Based on this figure, we can analyze the kinetics of the present system.

The HRP reaction with a soluble mediator is schematically represented as follows [23]:

$$\mathrm{HRP} + \mathrm{H_2O_2} \xrightarrow{k_1} \mathrm{Compound\ I} + \mathrm{H_2O} \quad (1)$$

$$\mathrm{Compound\ I} + \mathrm{Med(red)} \xrightarrow{k_2} \mathrm{Compound\ II} + \mathrm{Med(ox)} \quad (2)$$

$$\mathrm{Compound\ II} + \mathrm{Med(red)} \xrightarrow{k_3} \mathrm{HRP} + \mathrm{Med(ox)} \quad (3)$$

here k_1, k_2, and k_3 are rate constants, Med(red) and Med(ox) represent reduced and oxidized form of a soluble mediator, respectively, and Compounds I and II are the intermediate states of HRP, respectively. The kinetic equation of the overall reaction was derived as follows [7,24].

$$\frac{1}{v} = \frac{1}{k_1[\mathrm{H_2O_2}]} + \frac{k_2 + k_3}{k_2 k_3 [\mathrm{Med}]} \quad (4)$$

here v is the rate of the overall enzymatic reaction. In the present system containing no soluble mediator, the HRP intermediates, Compounds I and II, must accept electrons from the electrode through the AuNP core. Thus, the second term in the right hand of Eq. (4) is a constant depending on the electrode potential. Then, at a given electrode potential, Eq. (4) is redrawn as follows:

$$\frac{1}{v} = \frac{1}{k_1[\mathrm{H_2O_2}]} + \frac{1}{v_{\max}} \quad (5)$$

here $v_{\max}$ is a parameter including the rate constants of charge transfer between the HRP intermediates and the electrode, and represents the maximum rate under the condition of the sufficient substrate concentration. In addition, as the reactions take place only on the electrode, the observed surface reaction rate V in Fig. 6(B) depends on the surface density of HRP, Γ_E, according to the following relationship:

$$V = v\Gamma_E \quad (6)$$

In Fig. 6(B), the experimental data reasonably obey on the best fit curve (solid curve) based on the above formulations. From this analysis, we can calculate the maximum turnover as 30 s^{-1} using $\Gamma_E = 4.5 \times 10^{12}$ molecules cm^{-2} (estimated from preparative conditions).

As described in the foregoing section, the current response depended on the base electrode materials. Taking into account the above analysis using an Au disc electrode, we estimated the turnover of 70 s^{-1} for the case of the ITO base electrode. This value

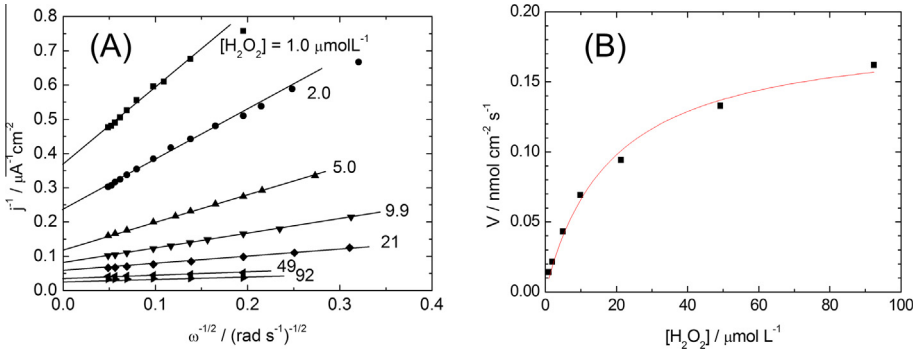

Fig. 6. Kinetic analysis using a hydrodynamic method. (A) Koutecky–Levich plots for the nanocomplex carrying Au-disc electrode at various H_2O_2 concentrations. (B) Surface reaction rate determined from (A) as a function of H_2O_2 concentration.

is order-of-magnitude higher than those of the related systems reported in the literatures [3,25].

We can discuss the effect of the base electrode materials on the sensor performance based on the above analysis. Returning to Fig. 3, all the curves bend to saturate in a similar H_2O_2 concentration region, although the responses are linear in a lower H_2O_2 concentration range and the sensitivity of the electrodes differs. According to the above kinetic analysis, this means that the specific activity of the enzyme itself is similar and only the effective amount of the enzyme differs among these electrodes. As the composition and the loaded density of the nanocomplex are identical in Fig. 3, the apparent difference in the enzyme amount is caused by the difference in the number of the nanocomplex that is electrically connected to the base electrode, that is, some parts of the nanocomplex immobilized on an electrode do not work – to be called "dead." Among the materials examined in this study, ITO is the best choice for minimizing the "dead" nanocomplexes, however, further exploration of the electrode materials or chemical modification of the electrode surfaces may improve this factor. The turnover frequencies above were calculated based on the loaded amount of HRP. However, taking into account the existence of the "dead" nanocomplexes, the "true" specific turnover for the "working" enzyme molecules may be higher, even in the case of an ITO base electrode.

3.4. Working potential

We again stress the mild working potential of the present system. We examined the working potential of the present system with cyclic voltammetry and the catalytic current measurement at constant potentials. The catalytic currents were observed from ca. +0.25 V vs. Ag/AgCl. Although the magnitude of the catalytic currents increased at more negative potentials, the background currents also increased at the more negative potentials. In view of both the catalytic sensitivity and the background stability, we concluded that the optimum potentials range from +0.15 to +0.20 V vs. Ag/AgCl. This potential range is similar to that of the electrode chemically immobilized HRP operated with ferrocene derivatives as the soluble mediator [7]. On the other hand, Xiao et al. [3] reported the catalytic direct electron transfer current through immobilized AuNP/adsorbed HRP system at −0.30 V vs. SCE, and Jia et al. [8] reported the working potential of −0.25 V vs. Ag/AgCl of the electrode carrying a silica gel network incorporating AuNPs and HRP. Ruzgas et al. [25] reported the catalytic current at −0.00 V vs. SCE for an HRP-modified graphite electrode. Comparing the potentials for these related systems, the present system features notably positive working potential for the effective electron transfer.

In the soluble mediator systems, Compounds I and II are reduced by the soluble mediator (electron donor) according to the above kinetic scheme (Eqs. (2) and (3)). Hexacyanoferrate(II) and ferrocene derivatives are well-known as the electron donor for HRP system [26]. The redox potential of these mediators is about +0.2 V vs. Ag/AgCl in neutral pH conditions, and the biosensor using the combination of HRP and these soluble mediators works at the potentials around this range [7,24,26]. In the present system, the sensor works at the similar potentials, and the direct electron transfer from the AuNP to Compounds I and II is as efficient as the typical soluble mediators. On the other hand, most of HRP–AuNP systems reported work at much negative potential such as −0.2 V vs Ag/AgCl [3,8–10]. Similar working potentials for the H_2O_2 detection were reported for an HRP-based nanowire system [27], nonenzymatic electrocatalytic systems [28–32], and nanomaterial-based systems with non-HRP proteins [13,33–37]. In these cases, it is reasonable to consider that the catalytic redox centers do not work according to the above scheme. In most of reported cases, H_2O_2 detection through direct electrochemistry of HRP (and related electrocatalysts) is not based on the native reaction of HRP, but another scheme utilizing Fe(II)-state of heme as demonstrated by the redox behavior of peroxidases [38,39].

3.5. Application to bienzyme systems

In spite of many reports about electrochemical biosensors using the HRP–AuNP combination, the present system features a noteworthy mild working potential, that is, the nanocomplex carrying electrode works at very mild potentials with minimized interference from co-existing electroactive species in practical samples. The present system is very suitable for monitoring the reaction by H_2O_2-generating enzymes – oxidases [7,26]. In view of this, two oxidases, glucose oxidase (GO) and urate oxidase (UO), were further immobilized on the nanocomplex-carrying electrode to fabricate sensors for glucose and uric acid, respectively. These enzymes catalyze the reaction between the corresponding substrate and dissolved oxygen to generate H_2O_2,

$$\text{Substrate} + O_2 \rightarrow \text{Oxidized substrate} + H_2O_2 \quad (7)$$

Fig. 7 shows the calibration curves of the sensors for glucose and uric acid. The working buffer was an air-saturated pH 6.4 phosphate buffer throughout, and all the operations were conducted at 25 °C under continuous stirring (~1 rps). The both electrodes reasonably responded to the corresponding substrates, respectively, and gave the steady-state current within 30 s.

The linear sensitivity of the glucose sensor in the low concentration region is in 0.1 μA mM^{-1} cm^{-2} level and is order-of-magnitude higher than that of 50 nA mM^{-1} cm^{-2} level for the electrode carrying HRP/GO bilayer operated with soluble mediators, that works with the identical principle [7]. The immobilized amounts of GO of the both sensors are in monolayer-modification level and estimated as in the same order. The sensitivity of the present system

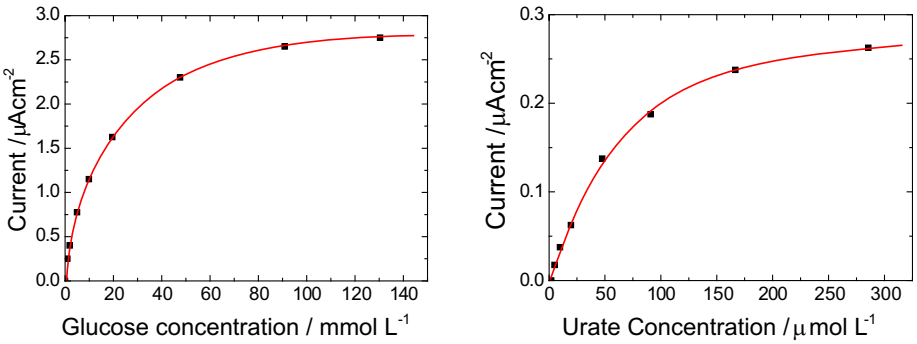

Fig. 7. Response of the bienzyme systems. Left, glucose oxidase; right, urate oxidase.

is based on the highly sensitive detection of H_2O_2 generated by the GO reaction. This is caused by the lack of loss of the Med(ox) reduction by diffusion to the solution bulk, and is a typical merit of non-mediator systems [40,41].

Although the detection of H_2O_2 is popular for GO-based electrochemical biosensors [7,42–44], the direct electrochemical detection of H_2O_2 generated by the UO reaction is generally difficult. H_2O_2 generated by the UO reaction readily forms a complex with allantoin, another product of the UO reaction [45], and the detection of free H_2O_2 is in principle limited [46]. Furthermore, the electrooxidation of H_2O_2 requires in general relatively high overpotentials and we can hardly avoid the direct electrooxidation of uricate itself that simultaneously occurs in the similar potential region. In view of this, Nanjo and Guilbault [46] employed electrochemical monitoring of O_2 consumption by the UO reaction for their historical UO-immobilized platinum electrode. However, the primary products of the UO reaction are reported as 5-hydroxyisourate and H_2O_2 [47], and a nonenzymatic post-reaction gives allantoin. Rapid and sensitive detection of primarily generated H_2O_2 may give a biosensor based on the detection of H_2O_2 just generated. Electrochemical detection of UO-generated H_2O_2 has been studied using several electrocatalysts [30]. Use of H_2O_2-specific enzyme may also dissolve this problem. Tatsuma et al. [26] employed an HRP/UO bilayer-modified electrode with a soluble mediator, and successfully detected the mediated reduction current of H_2O_2 generated by UO, however, the linear sensitivity in the low concentration region is limited to ca. 50 nA mM^{-1} cm^{-2}. The present nanocomplex-based urate sensor exhibited the sensitivity of ca. 3 μA mM^{-1} cm^{-2} in spite of the comparable amount of the immobilized enzyme, confirming order-of-magnitude higher detection efficiency of the present nanocomplex electrode.

3.6. Future scope

The present system demonstrates the facilitated electron transport between HRP and the base electrode through the AuNP as the nanoscale connector. This is probably related strongly to the adsorbed state of the enzyme molecules on the AuNP and some characteristic electronic interaction between the AuNP and the enzyme redox center (heme). In view of this, the examination of the size dependence of the AuNP on the sensor performance may give valuable information about the origin of the excellent charge transfer character of the present system.

It is also noteworthy that our system employs enzyme-nanoparticle nanocomplex that is spontaneously formed (a kind of self-assembly, in a way) as a functional unit. The nanocomplex can be easily immobilized to the electrode surface of many kinds of substrate materials and potentially compatible to some microfabrication technologies, such as ink-jet printing—the nanocomplex can be printed with an ink-jet printer at desired point or area, and applicable to fabricating printed devices.

Acknowledgement

We thank D. Fujii, N. Kouzaka, M. Nakagomi, and A. Sagara (Chiba Univ.) for their experimental assistance in part.

References

[1] J. Wang, Nanomaterial-based electrochemical biosensors, Analyst 130 (2005) 421.
[2] X. Luo, A. Morrin, A.J. Killard, M.R. Smyth, Application of nanoparticles in electrochemical sensors and biosensors, Electroanalysis 18 (2006) 319–326.
[3] Y. Xiao, H.-X. Ju, H.-Y. Chen, Direct electrochemistry of horseradish peroxidase immobilized on a colloid/cysteamine-modified gold electrode, Anal. Biochem. 278 (2000) 22–28.
[4] Y. Xiao, F. Patolsky, E. Katz, J.F. Hainfeld, I. Willner, "Plugging into Enzymes": nanowiring of redox enzymes by a gold nanoparticle, Science 299 (2003) 1877–1881.
[5] Y. Okawa, Y. Sakai, F. Shiba, Reagentless H_2O_2 biosensor with high electron transfer efficiency carrying nanocomplex of horseradish peroxidase and Au-nanoparticle, Electrochemistry 76 (2008) 522–524.
[6] K. Murata, M. Suzuki, K. Kajiya, N. Nakamura, H. Ohno, High performance bioanode based on direct electron transfer of fructose dehydrogenase at gold nanoparticle-modified electrodes, Electrochem. Commun. 11 (2009) 668–671.
[7] T. Tatsuma, Y. Okawa, T. Watanabe, Enzyme monolayer- and bilayer-modified tin oxide electrodes for the determination of hydrogen peroxide and glucose, Anal. Chem. 61 (1989) 2352–2355.
[8] J. Jia, B. Wang, A. Wu, G. Cheng, Z. Li, S. Dong, A method to construct a third-generation horseradish peroxidase biosensor: self-assembling gold nanoparticles to three-dimensional sol–gel network, Anal. Chem. 74 (2002) 2217–2223.
[9] S.-Q. Liu, H.-X. Ju, Renewable reagentless hydrogen peroxide sensor based on direct electron transfer of horseradish peroxidase immobilized on colloidal gold-modified electrode, Anal. Biochem. 307 (2002) 110–116.
[10] Q. Xu, C. Mao, N.-N. Liu, J.-J. Zhu, J. Sheng, Direct electrochemistry of horseradish peroxidase based on biocompatible carboxymethyl chitosan-gold nanoparticle nanocomposite, Biosens. Bioelectron. 22 (2006) 768–773.
[11] D. Shan, Q.-B. Li, S.-N. Ding, J.-Q. Xu, S. Cosnier, H.-G. Xue, Reagentless biosensor for hydrogen peroxide based on self-assembled films of horseradish peroxidase/laponite/chitosan and the primary investigation on the inhibitory effect by sulfide, Biosens. Bioelectron. 26 (2010) 536–541.
[12] M. Mathew, N. Sandhyarani, A novel electrochemical sensor surface for the detection of hydrogen peroxide using cyclic bisureas/gold nanoparticle composite, Biosens. Bioelectron. 28 (2011) 210–215.
[13] N. Wei, X. Xin, J. Du, J. Li, A novel hydrogen peroxide biosensor based on the immobilization of hemoglobin on three-dimensionally ordered macroporous (3DOM) gold-nanoparticle-doped titanium dioxide (GTD) film, Biosens. Bioelectron. 26 (2011) 3602–3607.
[14] J. Shen, X. Yang, Y. Zhu, H. Kang, H. Cao, C. Li, Gold-coated silica-fiber hybrid materials for application in a novel hydrogen peroxide biosensor, Biosens. Bioelectron. 34 (2012) 132–136.
[15] J. Turkevich, P.C. Stevenson, J. Hillier, A study of the nucleation and growth processes in the synthesis of colloidal gold, Discuss. Faraday Soc. 11 (1951) 55–75.
[16] J. Turkevich, P.C. Stevenson, J. Hillier, The formation of colloidal gold, J. Phys. Chem. 57 (1953) 670–673.
[17] G. Frens, Controlled nucleation for the regulation of the particle size in monodisperse gold suspensions, Nature 241 (1973) 20–22.
[18] D. Eck, C.A. Helm, N.J. Wagner, K.A. Vaynberg, Plasmon resonance measurements of the adsorption and adsorption kinetics of a biopolymer onto gold nanocolloids, Langmuir 17 (2001) 957–960.
[19] K.G. Welinder, Amino acid sequence studies of horseradish peroxidase. Amino and carboxyl termini, cyanogen bromide and tryptic fragments, the complete sequence, and some structural characteristics of horseradish peroxidase C, Eur. J. Biochem. 96 (1979) 483–502.
[20] C. Viebke, P.A. Williams, The influence of temperature on the characterization of water-soluble polymers using asymmetric flow field-flow-fractionation coupled to multiangle laser light scattering, Anal. Chem. 72 (2000) 3896–3901.
[21] T. Vegge, F.Ø. Winther, B.R. Olsen, Horseradish peroxidase in plasma studied by gel filtration, Histochemie 28 (1971) 16–22.
[22] M.B. Arnao, M. Acosta, J.A. del Río, R. Varón, F. García-Cánovas, A kinetic study on the suicide inactivation of peroxidase by hydrogen peroxide, Biochim. Biophys. Acta 1041 (1990) 43–47.
[23] H. Yamada, I. Yamazaki, Proton balance in conversions between five oxidation–reduction states of horseradish peroxidase, Arch. Biochem. Biophys. 165 (1974) 728–738.
[24] Y. Okawa, M. Nagano, S. Hirota, H. Kobayashi, T. Ohno, M. Watanabe, Tethered mediator biosensor. Mediated electron transfer between redox enzyme and electrode via ferrocene anchored to electrode surface with long poly(oxyethylene) chain, Biosens. Bioelectron. 14 (1999) 229–235.
[25] T. Ruzgas, L. Gorton, J. Emnéus, G. Marko-Varga, Kinetic models of horseradish peroxidase action on a graphite electrode, J. Electroanal. Chem. 391 (1995) 41–49.
[26] T. Tatsuma, T. Watanabe, Oxidase/peroxidase bilayer-modified electrodes as sensors for lactate, pyruvate, cholesterol and uric acid, Anal. Chim. Acta 242 (1991) 85–89.
[27] M.-J. Song, S.W. Hwang, D. Whang, Amperometric hydrogen peroxide biosensor based on a modified gold electrode with silver nanowires, J. Appl. Electrochem. 40 (2010) 2099–2105.
[28] X. Gao, L. Jin, Q. Wu, Z. Chen, X. Lin, A nonenzymatic hydrogen peroxide sensor based on silver nanowires and chitosan film, Electroanalysis 24 (2012) 1771–1777.
[29] W. Zhao, H. Wang, X. Qin, X. Wang, Z. Zhao, Z. Miao, et al., A novel nonenzymatic hydrogen peroxide sensor based on multi-wall carbon nanotube/silver nanoparticle nanohybrids modified gold electrode, Talanta 80 (2009) 1029–1033.
[30] W. Wang, C. Qin, Q. Xie, X. Qin, L. Chao, Y. Huang, et al., Rapid electrodeposition of a gold-Prussian blue nanocomposite with ultrahigh electroactivity for dual-potential amperometric biosensing of uric acid, Analyst 139 (2014) 2904–2911.

[31] C.M. Welch, C.E. Banks, A.O. Simm, R.G. Compton, Silver nanoparticle assemblies supported on glassy-carbon electrodes for the electro-analytical detection of hydrogen peroxide, Anal. Bioanal. Chem. 382 (2005) 12–21.
[32] M.R. Guascito, E. Filippo, C. Malitesta, D. Manno, A. Serra, A. Turco, A new amperometric nanostructured sensor for the analytical determination of hydrogen peroxide, Biosens. Bioelectron. 24 (2008) 1063–1069.
[33] W. Yang, Y. Li, Y. Bai, C. Sun, Hydrogen peroxide biosensor based on myoglobin/colloidal gold nanoparticles immobilized on glassy carbon electrode by a Nafion film, Sens. Actuators B Chem. 115 (2006) 42–48.
[34] C.-Y. Liu, J.-M. Hu, Hydrogen peroxide biosensor based on the direct electrochemistry of myoglobin immobilized on silver nanoparticles doped carbon nanotubes film, Biosens. Bioelectron. 24 (2009) 2149–2154.
[35] A. Safavi, F. Farjami, Hydrogen peroxide biosensor based on a myoglobin/hydrophilic room temperature ionic liquid film, Anal. Biochem. 402 (2010) 20–25.
[36] C. Liu, J. Hu, Direct electrochemistry of hemoglobin entrapped in composite electrodeposited chitosan-multiwall carbon nanotubes and nanogold particles membrane and its electrocatalytic application, Electroanalysis 20 (2008) 1067–1072.
[37] S. Liu, Z. Dai, H. Chen, H. Ju, Immobilization of hemoglobin on zirconium dioxide nanoparticles for preparation of a novel hydrogen peroxide biosensor, Biosens. Bioelectron. 19 (2004) 963–969.
[38] H.A. Harbury, Oxidation–reduction potentials of horseradish peroxidase, J. Biol. Chem. 225 (1957) 1009–1024.
[39] C.W. Conroy, P. Tyma, P.H. Daum, J.E. Erman, Oxidation–reduction potential measurements of cytochrome c peroxidase and pH dependent spectral transitions in the ferrous enzyme, Biochim. Biophys. Acta – Protein Struct. 537 (1978) 62–69.
[40] T. Tatsuma, T. Watanabe, Y. Okawa, Model analysis of enzyme monolayer- and bilayer-modified electrodes: the transient response, Anal. Chem. 64 (1992) 630–635.
[41] T. Tatsuma, T. Watanabe, Model analysis of enzyme monolayer- and bilayer-modified electrodes: the steady-state response, Anal. Chem. 64 (1992) 625–630.
[42] R.M. Ianniello, A.M. Yacynych, Immobilized enzyme chemically modified electrode as an amperometric sensor, Anal. Chem. 53 (1981) 2090–2095.
[43] T. Yao, A chemically-modified enzyme membrane electrode as an amperometric glucose sensor, Anal. Chim. Acta 148 (1983) 27–33.
[44] Y. Okawa, H. Tsuzuki, S. Yoshida, T. Watanabe, Glucose sensor carrying monomolecular layer covalently bound to tin(IV) oxide electrode, Anal. Sci. 5 (1989) 507–512.
[45] H.R. Mahler, G. Hübscher, H. Baum, Studies on uricase: I. Preparation, purification, and properties of a cuproprotein, J. Biol. Chem. 216 (1955) 625–642.
[46] M. Nanjo, G.G. Guilbault, Enzyme electrode sensing oxygen for uric acid in serum and urine, Anal. Chem. 46 (1974) 1769–1772.
[47] K. Kahn, P. Serfozo, P.A. Tipton, Identification of the true product of the urate oxidase reaction, J. Am. Chem. Soc. 119 (1997) 5435–5442.